

## RESEARCH ARTICLE

# Research on Seismic Acceleration Waveform Reproduction Based on Time-Frequency Hybrid Integration Algorithm

YING-QING GUO<sup>1</sup>, HAN-QI ZHANG<sup>1</sup>, YI-NA WANG<sup>1</sup>, AND JUN DAI<sup>2,3</sup><sup>1</sup>College of Mechanical and Electronic Engineering, Nanjing Forestry University, Nanjing 210037, China<sup>2</sup>China-Pakistan Belt and Road Joint Laboratory on Smart Disaster Prevention of Major Infrastructures, Southeast University, Nanjing 210096, China<sup>3</sup>School of Civil Engineering, Southeast University, Nanjing 210096, China

Corresponding author: Ying-Qing Guo (gyingqing@njfu.edu.cn)


This work was supported in part by the National Key Research and Development Programs of China under Grant 2019YFE0121900, in part by the National Natural Science Foundation of China under Grant 51878355 and Grant 52108442, and in part by the National Natural Science Foundation of China Key Projects under Grant 52130807.

**ABSTRACT** For the quadratic integration of seismic acceleration signal with noise and unknown initial velocity and displacement, the obtained displacement signal has serious trend error, which leads to the problem that the electrodynamic seismic simulation shaker under displacement control mode cannot accurately reproduce the seismic wave. This paper proposes the time-frequency hybrid integration algorithm based on time domain and frequency domain integration characteristics. The algorithm mainly includes two steps. The first step is to use the improved low-frequency attenuation algorithm to integrate the seismic acceleration for the first time in the frequency domain to obtain the corresponding velocity signal. The second step is to integrate the velocity signal directly in the time domain and combine it with the removal of the constant and linear terms algorithm to obtain the corresponding displacement signal. The accuracy and effectiveness of the algorithm are verified by numerical analysis and shaking table test. The results show that compared with the traditional hybrid integral algorithm, the performance improvement rates of displacement peak error and absolute error of the proposed time-frequency hybrid integral algorithm are 31.75% and 26.01%, respectively, and the accuracy of acceleration waveform reproduction is improved by 27.29%. Furthermore, when using this algorithm for the shaking table test of the seismic acceleration signal, the maximum peak error rate is only 4.92%. Therefore, this algorithm can effectively suppress the baseline drift and error accumulation caused by low-frequency noise and unknown initial state to realize the accurate reproduction of the acceleration waveform of the seismic simulation shaking table.

**INDEX TERMS** Time-frequency hybrid integration algorithm, seismic acceleration signal, removal of the constant and linear terms algorithm, improved low-frequency attenuation algorithm, electrodynamic seismic simulation shaker.

## I. INTRODUCTION

Earthquake is one of the major natural disasters, characterized by suddenness, destructiveness and unpredictability. Moreover, it seriously threatens the safety of human life and property, and it is usually accompanied by secondary disasters such as fire, tsunami, mudslides, and nuclear leakage to aggravate further the adverse effects of the disaster [1], [2].

The associate editor coordinating the review of this manuscript and approving it for publication was Chong Leong Gan .

At present, the accurate prediction technology for earthquakes is not perfect, so it is vital to improving the seismic performance of building structures to reduce the losses of earthquake disasters and protect people's lives and properties [3], [4]. However, due to the complexity of earthquake mechanism and structural seismic performance, it is difficult to truly understand the seismic performance under a natural earthquake environment only from theoretical analysis, so it must be studied in combination with experimental methods. The test methods widely used for the seismic performance of

structures are mainly the proposed dynamic test method [5], the pseudo-static test method [6], and the seismic simulated shaking table test method [7], [8], [9]. The seismic simulated shaking table test can visualize the structure's seismic performance under seismic wave excitation, so the seismic simulated shaking table test method has become the most common method to study the seismic performance of structures [10], [11]. In the displacement control mode, the input signal of the seismic simulation shaking table is the displacement signal. At the same time, the seismic wave information is mainly stored as acceleration signal [12], [13], so it is important to convert the seismic acceleration signal into displacement signal in the shaking table test. Since the integration of seismic acceleration is disturbed by the trend term error, the integrated displacement curve is severely shifted and cannot meet the engineering requirements. Therefore, eliminating the error trend term in the integration process of seismic acceleration signal has become a hot research topic.

For the problems faced in reconstructing displacement signals from acceleration signals, the mainstream methods include the time domain integration method [14], [15] and the frequency domain integration method [16], [17], [18]. Chen [15] *et al.* offered a method to fit the integrated displacement waveform by a polynomial, subtracting the fitted polynomial from the integrated out displacement to remove the trend term. This method can sufficiently reduce the errors caused by the unknown initial velocity and displacement and the DC errors. However, the effect of low-frequency noise on the integration accuracy is difficult to control, so the method has no suitable engineering applications. The low-frequency cutoff algorithm [19], [20] reconstructs the displacement from the measured acceleration. The low-frequency cutoff algorithm first performs the fast Fourier transform on the acceleration signal, then sets the low-frequency signal below the cutoff frequency directly to zero for frequency domain integration, and then reconstructs the displacement using the inverse fast Fourier transform. This algorithm can eliminate the low-frequency noise below the selected cutoff frequency. However, the effective low-frequency signals are also removed, and the cutoff frequency selection is highly subjective and empirical. Zhang [21] proposed an integration algorithm based on the Walsh transform and empirical modal decomposition, which does not need to specify key parameters such as cutoff frequency and target frequency. However, because the empirical modal decomposition has the disadvantage of modal confusion, there is also a certain error in removing low-frequency noise simultaneously. In addition to the mainstream methods nowadays, many researchers have submitted various algorithms to improve the accuracy of the acceleration after secondary integration. Lotfi [22] proposed that the noise of the acceleration signal is removed through a smoothing process based on a diffusion equation, a special partial differential equation. However, this method is only applicable to the localized signal deviation that is more obvious. Kong [23] proposed a stabilized numerical integration

method for acceleration sensor data processing. This method is for relatively stable acceleration, while the seismic acceleration signal amplitude changes rapidly, so the applicability is not strong. By constructing a strict system to modify the transfer function of the integration system, the drift of the acceleration data after secondary integration is effectively suppressed. Liu [24] suggested the non-integral displacement reconstruction method using complex exponential series to establish the relationship between measured acceleration and target displacement. Nevertheless, this method has subjective knowledge about establishing complex exponential series of acceleration. Ansari [25] presented a wavelet denoising method to eliminate errors and compared it in time domain integration and frequency domain integration, but wavelet denoising has to select the corresponding cutoff frequency whose subjectivity is strong. Guo [26] proposed a hybrid integration algorithm combining frequency domain and time domain integration to control the error trend term of the integration process. Since its time domain integration uses the least-squares method to remove the linear error term, it does not consider the presence of any constant error term after the quadratic integration.

Most of the above algorithm controls the error trend term of the integration mainly by discarding part of the low-frequency information of the acceleration signal. In contrast, for the seismic acceleration signal, the effective frequency band is mainly concentrated in the middle and low frequencies (0~15Hz). The effective seismic acceleration signal will be affected using the algorithm above to eliminate the error trend term. Meanwhile, most researchers assume zero for the initial state of velocity and displacement, which cannot be considered in the practical application. In order to better retain the effective information of displacement after integration and at the same time improve the accuracy of reconstructed displacement signal of seismic acceleration signal and the accuracy of seismic simulation shaker reproduction in displacement control mode, this paper proposes a time-frequency hybrid integration algorithm by analyzing the source of reconstruction displacement error, the characteristics of frequency domain integration and time domain integration. The first integration of the time-frequency hybrid integration algorithm adopts the improved low-Frequency attenuation algorithm in the frequency domain to obtain the corresponding velocity signal; the second integration adopts the time-domain integration and combines the removal of the constant and linear terms algorithm to obtain the corresponding displacement signal. The numerical analysis and shaker tests show that the performance improvement rate of peak displacement error and absolute error obtained under time-frequency hybrid integration algorithm processing is 31.75% and 26.01% compared with the traditional hybrid integration algorithm; the acceleration waveform reproduction accuracy is improved by 27.29%. The maximum peak error rate for the 110Gal El Centro actual seismic acceleration signal replication is only 4.92%, which meets the engineering requirements. The research results are of great practical significance

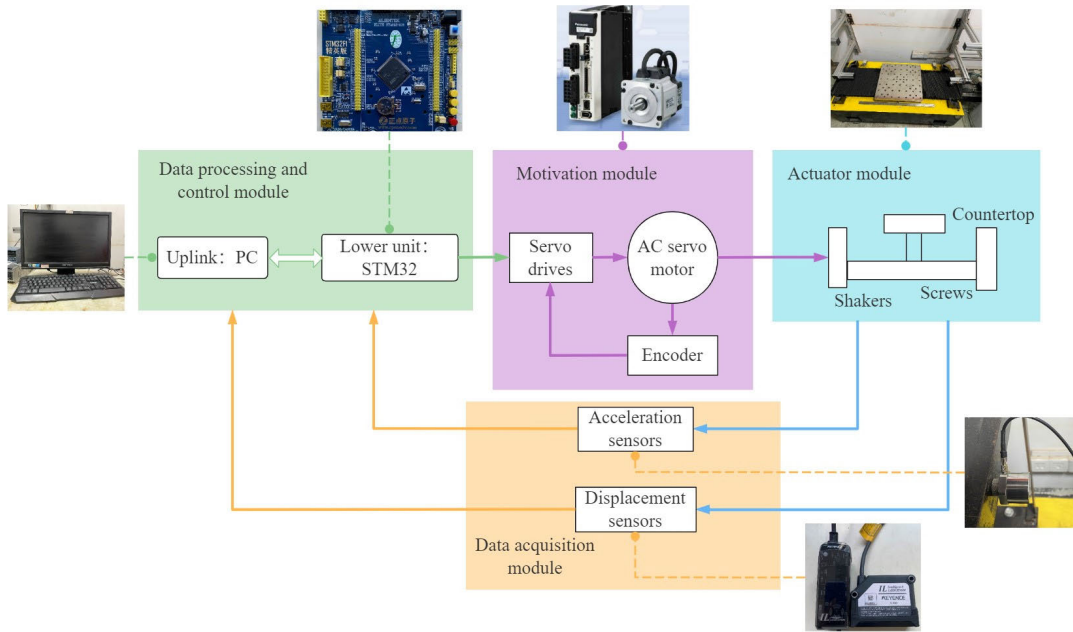


FIGURE 1. The Structure diagram of electrodynamic seismic simulation shaker test device.

in exploring the seismic performance of building structures and broadening the application fields of shakers.

## II. STRUCTURE OF ELECTRODYNAMIC SEISMIC SIMULATION SHAKER

The project team and Professor Zhao-Dong Xu’s team at Southeast University independently developed a single degree of freedom small and medium-sized, high-precision electrodynamic seismic simulation shaker test device based on STM32 control. The overall system structure is shown in Fig. 1. The vibration table adopts an AC servo motor as the actuator, and its control mode is displacement control mode. In this control mode, the upper computer is used to process the original data of seismic acceleration and reconstruct the displacement signal. Then the displacement signal is converted into the drive signal-pulse signal of the servo drive by the lower computer to realize the real-time control of the rotational speed and the positive and negative rotation of the servo motor and promote the accurate movement of the vibration table. At the same time, the laser displacement sensor and the acceleration sensor are used to collect the table’s vibration displacement and acceleration signals to facilitate the subsequent performance analysis of the vibration table.

## III. PROCESSING OF SEISMIC ACCELERATION SIGNALS

### A. PROBLEM ANALYSIS

Since the electrodynamic seismic simulation shaker in this paper uses the displacement control mode, and the seismic acceleration signal reconstructs the displacement when an error trend term is generated, which results in the reproduction accuracy of the shaker cannot be guaranteed. There are two main reasons for the trend term error: one is the

introduction of a certain amount of low-frequency noise in the seismic acceleration signal acquisition [27]; the other reason is the unknown initial displacement and initial velocity in the acquired acceleration signal. These factors lead to the accumulation of errors in the integration process, resulting in a displacement error trend term.

The first reason is due to the irresistible factors of the acquisition equipment and the acquisition environment. For the second reason to be studied and analyzed. Suppose the acceleration signal without low-frequency noise is  $a(t)$ , then the corresponding velocity  $V(t)$  and displacement  $X(t)$  are theoretically defined as the first and second time integration of  $a(t)$ , respectively, as:

$$V(t) = \int_0^t a(\tau) d\tau = v(\tau) \Big|_0^t = v(t) - v(0) \quad (1)$$

and

$$X(t) = \int_0^t V(\tau) d\tau = x(t) - \mu(t) \quad (2)$$

where  $\mu(t)$  is the linear error component,  $\mu(t) = v(0)t + x(0)$ ;  $v(0)$  and  $x(0)$  are the initial velocity and displacement, respectively;  $v(t)$  and  $x(t)$  are the ideal velocity and displacement. From equation (2), it can be seen that the displacement signal obtained after quadratic integration of the acceleration signal in the time domain can be divided into two parts: the first part is the ideal displacement, and the second part consists of the initial conditions.

Since the initial conditions  $x(0)$  and  $v(0)$  are unknown, the exact displacement cannot be obtained after integrating the acceleration signal twice in the time domain. So the linear error component  $\mu(t)$  needs to be eliminated to get the ideal

displacement  $x(t)$ . For example, suppose the acceleration signal  $a(t)$  is:

$$a(t) = 1.1 \sin(t), \quad 0 \leq t \leq 10 \quad (3)$$

The image of  $a(t)$  is shown in Fig. 2(a). The velocity signal  $V(t)$  obtained by one time domain integration of the acceleration signal  $a(t)$  is shown in Fig. 2(b). The baseline of the velocity signal curve is not at the zero point, as can be seen in Fig. 2(b). The displacement signal  $X(t)$  obtained by one time domain integration of the velocity signal  $V(t)$  is shown in Fig. 2(c). The displacement signal curve in Fig. 2(c) undergoes an apparent linear drift phenomenon.

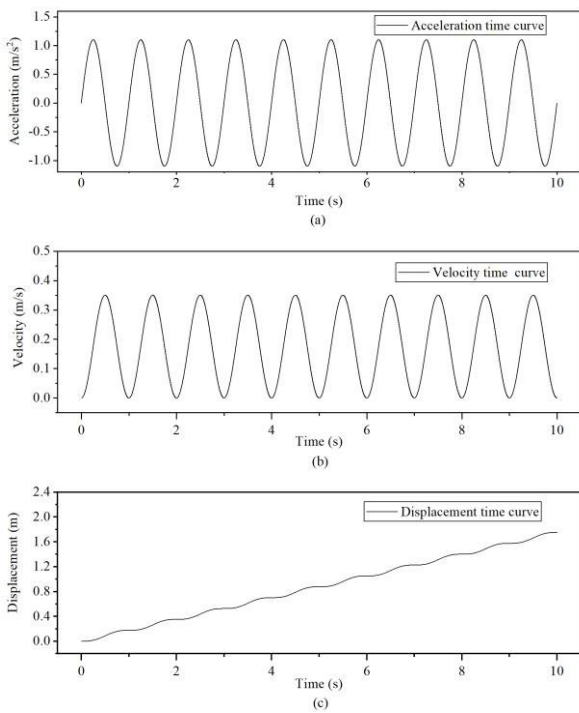


**FIGURE 2.** Baseline drift phenomenon of acceleration data: (a) The curve of acceleration signal; (b) The curve of velocity signal; (c) The curve of displacement signal.

### B. PROBLEM HANDLING

1) IMPROVED LOW-FREQUENCY ATTENUATION ALGORITHM  
An improved low-frequency attenuation algorithm [16] is used to process the seismic acceleration signal's low-frequency noise. This algorithm integrates the seismic acceleration signal containing low-frequency noise directly in the frequency domain, using the target accuracy factor  $\alpha_T$  to ensure the integration accuracy while eliminating the filter design link, simplifying the integration process, and avoiding filter frequency domain oscillations.

Transforming the noise acceleration signal  $\bar{a}(t)$  into displacement  $\bar{s}(t)$  using the summation function and

Fourier transform:

$$\begin{cases} \mathcal{F}(\bar{s}(t)) = H_E(\omega) \mathcal{F}(\bar{a}(t)) = -\frac{1}{\omega^2} \mathcal{F}(\bar{a}(t)) \\ \bar{s}(t) = -\mathcal{F}^{-1} \left[ \frac{1}{\omega^2} \mathcal{F}(\bar{a}(t)) \right] \end{cases} \quad (4)$$

where  $H_E(\omega)$  is the exact transfer function of  $\bar{s}(t)$  concerning  $\bar{a}(t)$  and  $\omega$  is the angular frequency.

Since the above-reconstructed displacement  $\bar{s}(t)$  still has noise content, the acceleration reconstruction of the displacement is now carried out through the inverse problem, and this inverse problem reconstructs the displacement by solving the minimum value problem of equation (5) [18]:

$$\min \prod(s) = \frac{\beta^2}{2} \int_{T_1}^{T_2} s^2 dt + \frac{1}{2} \int_{T_1}^{T_2} \left( \frac{d^2 s}{dt^2} - \bar{a} \right)^2 dt \quad (5)$$

The first term is the regularization function used to restrain the discomfort and rank loss of the inverse problem, and  $\beta$  is the regularization factor to adjust the regularization effect in the displacement reconstruction process. The second term is used to control the approximation of the integration process to the test acceleration. By solving the dual-objective optimization problem of equation (5), the frequency response function  $H_B(f)$  between the input noise acceleration  $\bar{a}(t)$  and the output displacement  $\bar{s}(t)$  is derived as:

$$H_B(f) = -\frac{\omega^2}{\omega^4 + \beta^2} = -\frac{(2\pi f)^2}{(2\pi f)^4 + \beta^2} \quad (6)$$

where  $f$  is the frequency. Since the displacement can be explained by the Fourier transform and the Fourier inverse transform:

$$\begin{cases} \mathcal{F}(\bar{s}(t)) = H_B(f) \mathcal{F}(\bar{a}(t)) \\ \bar{s}(t) = \mathcal{F}^{-1} [H_B(f) \mathcal{F}(\bar{a}(t))] \end{cases} \quad (7)$$

Assuming that  $\hat{a}(t) = \frac{d^2 \bar{s}}{dt^2}$  is the output acceleration, the frequency response function  $H_B^{acc}(f)$  between the output acceleration  $\hat{a}$  and the input acceleration  $\bar{a}$  is:

$$H_B^{acc}(f) = \frac{H_B(\omega)}{H_E(\omega)} = \frac{\omega^4}{\omega^4 + \beta^2} = \frac{(2\pi f)^4}{(2\pi f)^4 + \beta^2} \quad (8)$$

The target frequency  $f_T$  is introduced in accordance with the fundamental frequency of the noise acceleration, and equation (6) and (8) are normalized:

$$\begin{cases} H_B(\tilde{f}) = \frac{H_B(f)}{\frac{1}{(2\pi f_T)^2}} = -\frac{\tilde{f}^2}{\left[ \tilde{f}^4 + \frac{\beta^2}{(2\pi f_T)^4} \right]} \\ H_B^{acc}(\tilde{f}) = \frac{\omega^4}{\omega^4 + \beta^2} = \frac{\tilde{f}^4}{\left[ \tilde{f}^4 + \frac{\beta^2}{(2\pi f_T)^4} \right]} \end{cases} \quad (9)$$

where  $\tilde{f}$  is the normalized frequency and  $\tilde{f} = f/f_T$ ; when the frequency  $f = f_T$ , the value of  $\tilde{f}$  is 1. Define  $H_B(\tilde{f})$  as the target accuracy factor  $\alpha_T$  at this point:

$$\alpha_T = \frac{1}{1 + \frac{\beta^2}{(2\pi f_T)^4}}, \quad 0 \leq \alpha_T \leq 1 \quad (10)$$



the regularization factor  $\beta$  can be derived by equation (10):

$$\beta^2 = \frac{(2\pi f_T)^4}{\alpha_T} - (2\pi f_T)^4 \quad (11)$$

Substituting equation (11) into equation (9) yields the normalized frequency response function between the input noise acceleration  $\bar{a}$  and the output displacement  $\bar{s}$  and between the input noise acceleration  $\bar{a}$  and the output acceleration  $\hat{a}$ :

$$\begin{cases} H_B(\tilde{f}) = -\frac{\tilde{f}^2}{(\tilde{f}^4 - 1 + \frac{1}{\alpha_T})} \\ \&H_B^{acc}(\tilde{f}) = \frac{\tilde{f}^4}{(\tilde{f}^4 - 1 + \frac{1}{\alpha_T})} \end{cases} \quad (12)$$

From equation (12), it can be seen that the phase difference corresponding to the input noise acceleration  $\bar{a}$  and the output displacement  $\bar{s}$  is a constant value  $\pi$ , and the phase difference between the input noise acceleration  $\bar{a}$  and the output acceleration  $\hat{a}$  is 0; the value of  $\alpha_T$  determines the accuracy of the whole reconstructed displacement at this time.

An improved low-frequency attenuation algorithm is proposed based on the amplitude-frequency characteristics of the input noise acceleration signal and the output displacement. The algorithm achieves trend term error control by attenuating the low-frequency information in the input noise acceleration signal in the frequency domain; it can effectively retain the information near the signal  $f_T = 1$ , and substantially attenuate the ultra-low-frequency information far from  $f_T$  to achieve both the full consideration of trend term error control and the effective information retention purpose. When the target accuracy factor  $\alpha_T$  is 1, the amplitude and frequency characteristics of the algorithm are consistent with the direct frequency domain integration algorithm, and there is no trend term error control effect. When the value of  $\alpha_T$  is higher, the low-frequency components are suppressed significantly, and the trend term error caused by low-frequency noise is controlled better. As the integration accuracy  $\alpha_T$  decreases, the degree of attenuation of low-frequency information increases, and the suppression of the integration trend term error increases; however, it also increases the attenuation of the input signal amplitude. Therefore, this algorithm  $\alpha_T$  should be selected according to the degree of low-frequency noise in the signal and the trend term error control based on the largest possible value (in this paper,  $\alpha_T = 0.99$ ), so that the effective information in the signal is fully retained.

Also, using the same idea as above, the transfer function  $H_c(f)$  between the input noise acceleration  $\bar{a}$  and the output velocity  $\bar{v}$  can be analogously derived as:

$$H_c(f) = \frac{\omega}{\omega^2 + \beta^2} = \frac{2\pi f}{(2\pi f)^2 + \beta^2} \quad (13)$$

normalize equation (13):

$$H_c(\tilde{f}) = \frac{H_c(f)}{\frac{1}{2\pi f_T}} = \frac{\tilde{f}}{(\tilde{f}^2 - 1 + \frac{1}{\alpha_T})} \quad (14)$$

The noise acceleration  $\bar{a}$  is reconstructed into velocity  $\bar{v}$  using equation (14), and the steps are shown in Fig. 3.

## 2) REMOVAL OF CONSTANT AND LINEAR TERMS ALGORITHM

For the case where the initial conditions  $x(0)$  and  $v(0)$  are unknown, thus causing a zero-point drift in the secondary integration of the seismic acceleration signal, this paper proposes the removal of constant and linear terms algorithm. This algorithm eliminates the constant error term after each time domain integration so that the linear error term will not be generated when the second time-domain integration is performed. The ideal displacement can be obtained using this algorithm.

It must be clear that the source of the error after the direct time integration is the constant error term  $v(0)$ , and the source of the error after secondary integration is the linear error term  $v(0)t$  and the constant error term  $x(0)$ . After the direct time integration, the constant error term is fused with the whole expression. At the same time, it can be determined that there will be no other constant term other than the constant error term in the whole expression, so remove the constant term from the expression. The following is an analysis of the principle of removing the constant term from the expression.

Bringing the constant error term  $v(0)$  into the Fourier transform formula  $F(\omega) = \int_{-\infty}^{+\infty} y(t) e^{-j\omega t} dt$  yields:

$$\mathcal{F}(\omega) = \int_{-\infty}^{+\infty} v(0) e^{-j\omega t} dt = v(0) \int_{-\infty}^{+\infty} e^{-j\omega t} dt \quad (15)$$

Let  $\int_{-\infty}^{+\infty} e^{-j\omega t} dt = z$ . Since  $z$  is a generalized integral, the equation (15) is calculated by the substitution method. Take  $\delta(t)$  and bring it into the Fourier transform formula to get:

$$\mathcal{F}(\omega) = \int_{-\infty}^{+\infty} \delta(t) e^{-j\omega t} dt \quad (16)$$

where  $\delta(t)$  is the unit pulse signal, find  $\mathcal{F}(\omega) = 1$ , and Fourier inversion of equation (16) yields:

$$\delta(t) = \frac{1}{2\pi} \int_{-\infty}^{+\infty} 1 * e^{j\omega t} d\omega \quad (17)$$

replacing  $t$  in equation (17) with  $-\omega$  gives:

$$2\pi * \delta(-\omega) = \int_{-\infty}^{+\infty} e^{-j\omega t} dt \quad (18)$$

substituting equation (18) into equation (15) yields:

$$\mathcal{F}(\omega) = v(0) * 2\pi * \delta(\omega) \quad (19)$$

As can be seen from equation (19), the constant error term obtained after the time domain integration of the acceleration signal only affects the amplitude in the frequency domain when  $\omega = 0$ . Therefore, after the direct time domain integration of the acceleration signal, the Fourier transform is first performed, and then the amplitude in the frequency domain when  $\omega = 0$  is zero. Finally, the Fourier inverse transform is used to transform the corrected velocity signal in the frequency domain into the time domain velocity signal.

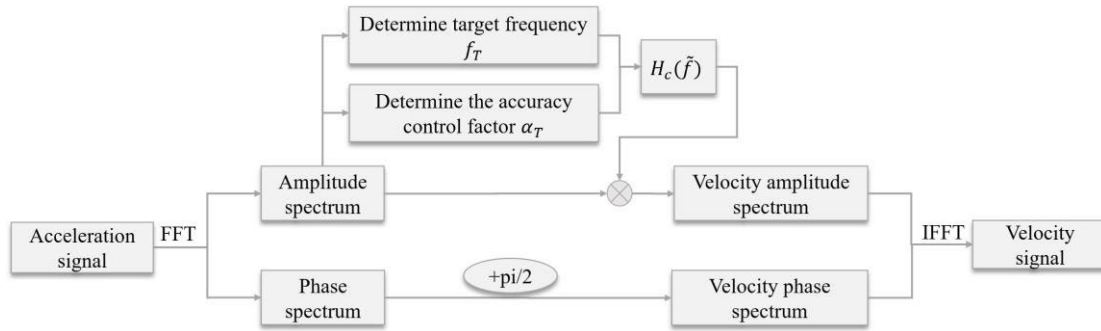


FIGURE 3. Flow chart of reconstructing velocity signal from the.

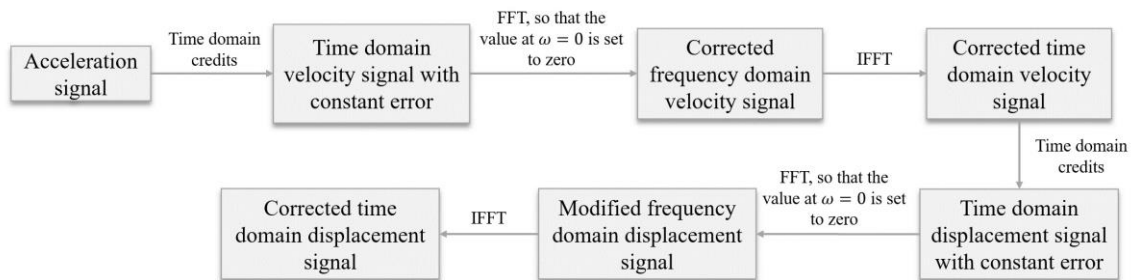


FIGURE 4. Flow chart of reconstructing velocity signal from the noisy acceleration signal.

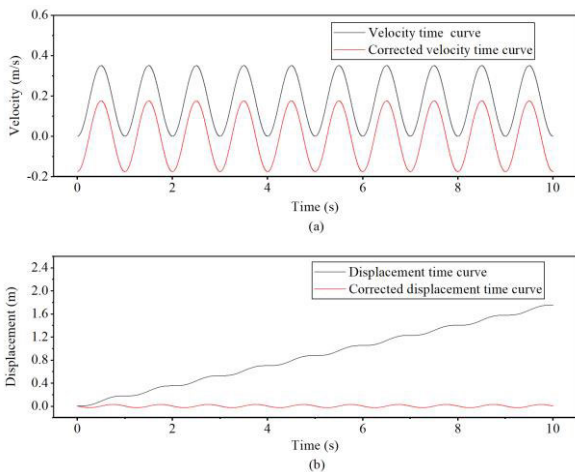


FIGURE 5. Corrected comparison diagram: (a)Velocity comparison diagram; (b)Displacement comparison diagram.

In the second integration of the resulting constant error term, the same processing method can be used to obtain the ideal displacement. The flow chart of the removal of constant and linear terms algorithm is shown in Fig. 4. This algorithm is applied to the seismic acceleration signal  $a(t)$  shown in equation (3). The corrected velocity and displacement time curves are shown in Fig. 5. As can be seen from Fig. 5, this

algorithm accurately and effectively eliminates the constant and linear error trend terms after quadratic integration.

### 3) TIME-FREQUENCY HYBRID INTEGRATION ALGORITHM

For the seismic acceleration signal containing low-frequency noise and an unknown initial state for displacement reconstruction, while considering that the cumulative error generated by the second integration in the time domain is more significant than that of the first integration, and the second integration in the frequency domain is influenced by the low-frequency error than that of the first integration, this paper designs the time-frequency hybrid integration algorithm. First, the velocity signal is obtained by integrating the acceleration signal with low-frequency noise once in the frequency domain using the improved low-frequency attenuation integration algorithm. This process can reduce the influence of low-frequency noise on the velocity reconstruction while using the constant removal and linear term algorithm to process the velocity signal. Then, the velocity signal is integrated once using the time domain integration to obtain the displacement signal containing the error term. Finally, the ideal displacement signal is obtained by correcting the displacement signal with the error term using the removal of constant and linear terms algorithm. The flow chart of the time-frequency hybrid integration algorithm is shown in Fig. 6. The traditional hybrid integration algorithm uses

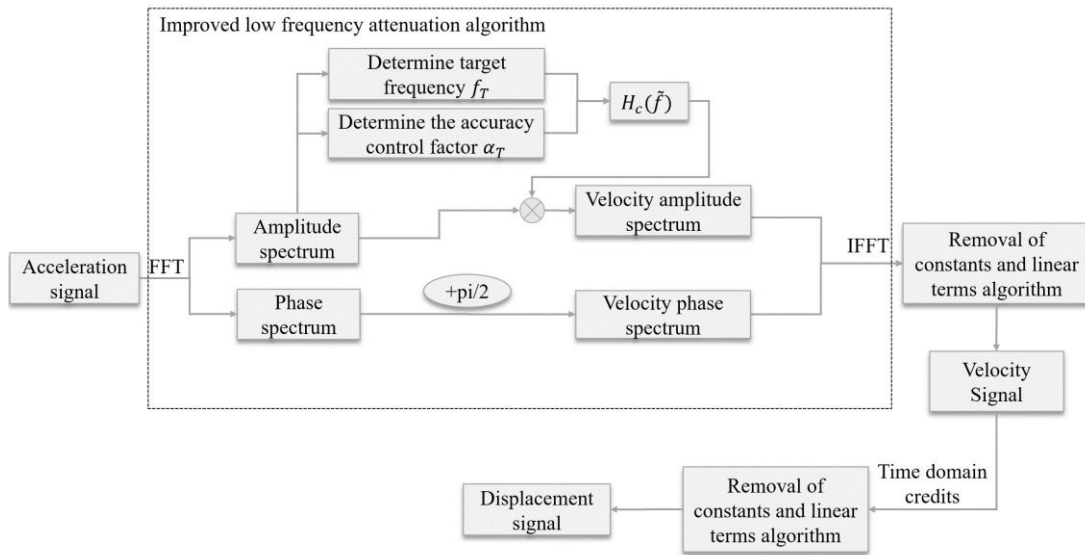


FIGURE 6. Flow chart of time-frequency hybrid integration algorithm.

a least squares algorithm for the second integration to eliminate the linear trend term, and this time-frequency hybrid integration algorithm can remove the constant and linear error more accurately and achieve displacement reconstruction better.

In numerical simulation to validate the superiority of the time-frequency hybrid integration algorithm, the simulated signal is a sinusoidal signal containing Gaussian white noise with an amplitude of  $1\text{m/s}^2$  and a frequency of  $15\text{Hz}$ . This signal is similar to the real seismic wave in frequency characteristics and noise level, and its signal is shown in Fig. 7(a). By comparing the Polynomial Fitting (PF) algorithm, the Improve Low-frequency Attenuation (ILFA) algorithm, and the Traditional Hybrid Integration (THI) algorithm to prove that the Time-frequency Hybrid Integration (TFHI) Algorithm can further improve the displacement accuracy after quadratic integration. The theoretical analysis shows that the velocity signal should be a cosine signal with an amplitude of  $-1/30\pi\text{m}$  and frequency of  $15\text{Hz}$ , and the displacement should be a sine signal with an amplitude of  $-1/(0.9\pi^2)\text{mm}$  and frequency of  $15\text{Hz}$ . After data processing, the error of the velocity signal after one integration is not very large, as can be seen from the velocity comparison graph in Fig. 7(b). The displacement comparison graph in Fig. 7(c) and the displacement error graph in Fig. 8 show that the displacement obtained by different integration algorithms differs more obviously. When the time-frequency hybrid integration algorithm is used, the displacement error is controlled within  $-0.05$  to  $0.025\text{mm}$ , which is more closely matched to the ideal displacement signal. According to the characteristics of the vibration signal, the peak error (ERP) and absolute error (ERS) of displacement after integration of different algorithms are calculated, and the equation is shown in

equation (20) and equation (21).

$$\text{ERP} = \frac{1}{2} \left\{ \left| \frac{\max [s_0(t)] - \max [s(t)]}{\max [s(t)]} \right| + \left| \frac{\min [s_0(t)] - \min [s(t)]}{\min [s(t)]} \right| \right\} \quad (20)$$

and

$$\text{ERS} = \frac{\sum_{i=1}^N |s_0(t) - s(t)|}{\sum_{i=1}^N |s(t)|} \quad (21)$$

The smaller the ERP and ERS, the more accurate the integration result. In order to reflect advantages of the time-frequency hybrid integration algorithm, define the performance improvement  $R_{\text{ERP}}$  and  $R_{\text{ERS}}$  of this algorithm for the displacement ERP and ERS of the conventional algorithm, which are calculated as:

$$\begin{cases} R_{\text{ERP}} = \frac{A_{\text{ERP}} - I_{\text{ERP}}}{I_{\text{ERP}}} \times 100\% \\ R_{\text{ERS}} = \frac{A_{\text{ERS}} - I_{\text{ERS}}}{I_{\text{ERS}}} \times 100\% \end{cases} \quad (22)$$

where  $A_{\text{ERS}}$  and  $I_{\text{ERS}}$  are the displacement ERP and ERS of various conventional integration algorithms, respectively;  $I_{\text{ERP}}$  and  $I_{\text{ERS}}$  are the displacement ERP and ERS of time-frequency hybrid integration algorithms, respectively. Higher values of  $R_{\text{ERP}}$  and  $R_{\text{ERS}}$  indicate more significant performance improvement. Table 1 shows the simulated signal's displacement ERP and ERS under different integration algorithms. Table 1 shows the performance improvement rate  $R_{\text{ERP}}$  and  $R_{\text{ERS}}$  of the time-frequency hybrid integration algorithm compared with the corresponding traditional integration algorithm. The data analysis in Tables 1 and 2 shows that the ERP and ERS of the time-frequency hybrid integration algorithm are reduced compared with the traditional

**TABLE 1.** The displacement peak error (ERP) and absolute error (ERS).

Algorithm	ERP	ERS
PF	0.362	0.608
ILFA	0.376	0.552
THI	0.278	0.344
TFHI	0.211	0.273

**TABLE 2.** The performance improvement rate  $R_{ERP}$  and  $R_{ERS}$  of the time-frequency hybrid integration algorithm.

Algorithm	$R_{ERP}$	$R_{ERS}$
PF	71.56%	122.71%
ILFA	78.20%	102.20%
THI	31.75%	26.01%

hybrid integration algorithm, and the performance improvement rates of  $R_{ERP}$  and  $R_{ERS}$  are 31.75% and 26.01%, respectively. In summary, the time-frequency hybrid integration algorithm can further improve the integration accuracy of seismic acceleration signals.

**IV. SHAKING TABLE TEST**

To verify the practical effect of the time-frequency hybrid integration algorithm proposed in this paper, the test was conducted in combination with the electrodynamic seismic simulation shaker test device described above, and the test device is shown in Fig. 9. Firstly, verify that the performance of this device meets the test requirements by testing the test device. Secondly, the superiority and accuracy of the time-frequency hybrid integration algorithm are confirmed through the acceleration waveform reproduction test with different integration algorithms. Finally, the actual seismic acceleration waveform is used for the reproduction test to prove the reliability of this algorithm.

**A. TEST DEVICE TESTING**

The electrodynamic shaker’s control effect directly affects the seismic wave reproduction accuracy. To verify the device system’s good control performance, this shaker’s control effect is judged by the reproduction degree of input and output displacement. The displacement signal was obtained by quadratic integration of the 110Gal El Centro acceleration signal. The displacement data was converted into pulse signals and input to the seismic simulation shaker system. Finally, the high-precision laser displacement sensor collected the shaker output displacement signal for comparison with the input displacement signal. The comparison graph of the displacement input signal and output signal is shown in Fig. 10, from which it can be seen that the output displacement signal is basically the same as the input signal. The input and output displacement error is calculated through the equation (23). The displacement error graph is shown in Fig. 11. The highest value of displacement error appears in

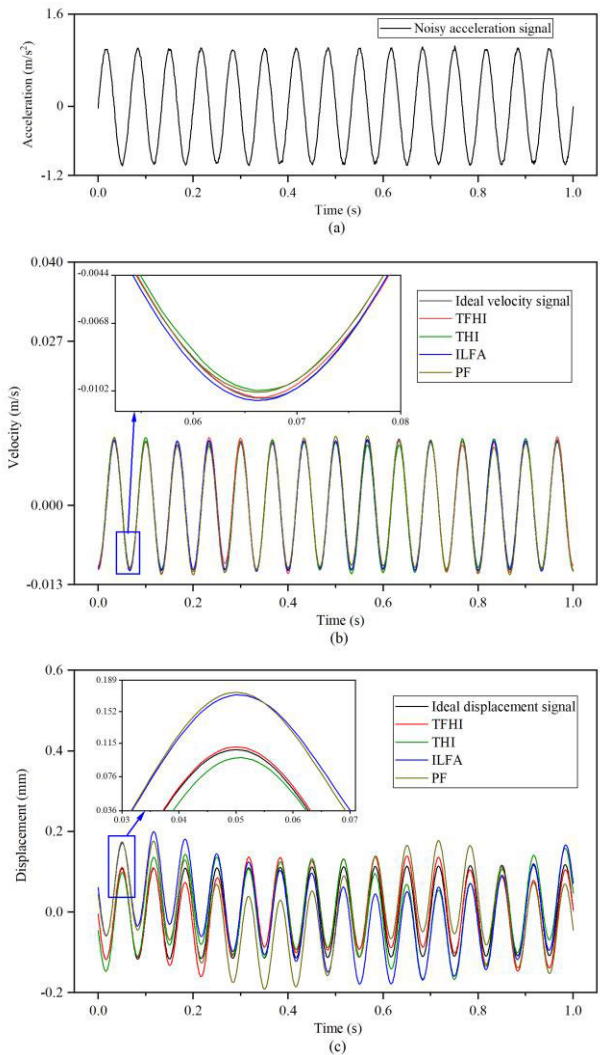


**FIGURE 7.** Comparison of data processing of different algorithms for 1m/s<sup>2</sup> sinusoidal signal with noise: (a) 1m/s<sup>2</sup> noisy acceleration signal; (b) velocity comparison diagram; (c) displacement comparison diagram.

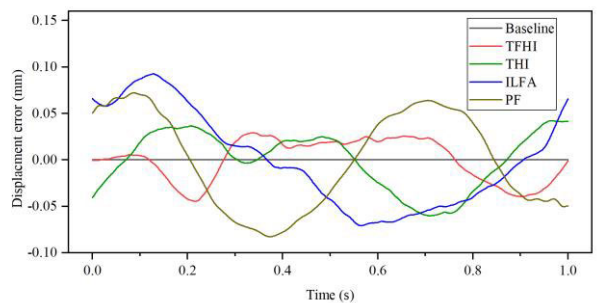


**FIGURE 8.** Displacement error diagram after data processing of 1m/s<sup>2</sup> sinusoidal signal with noise.

26.20s as 3.22mm, and the displacement error value  $Err_{dis}$  is mainly concentrated in the -2mm to 2mm interval. Using the equation (24) analysis, the peak error of the measured displacement  $ERP_{dis}$  is 0.003247. This shaker displacement



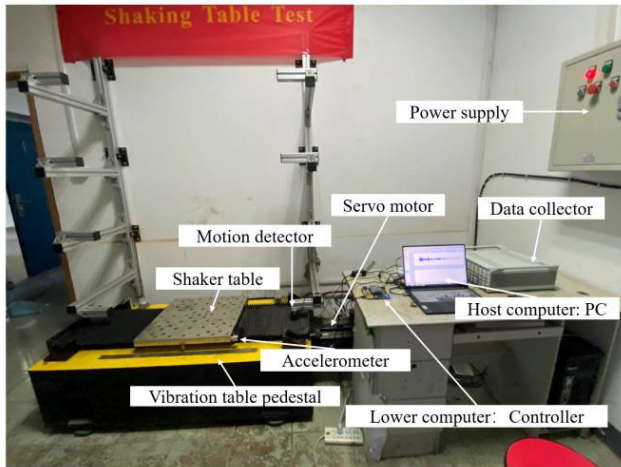


FIGURE 9. Electrodynamic seismic simulation shaker test device.

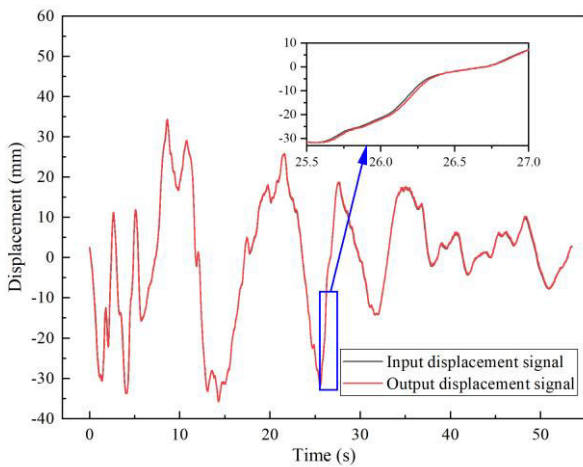


FIGURE 10. Comparison of displacement input and output of 110Gal El Centro wave.

reproduction accuracy is high the performance meets the engineering requirements.

$$Err_{dis} = X_r(t) - X_c(t) \quad (23)$$

where  $X_r(t)$  is the input displacement and  $X_c(t)$  is the output displacement.

$$ERP_{dis} = \frac{1}{2} \left\{ \left| \frac{\max [X_r(t)] - \max [X_c(t)]}{\max [X_c(t)]} \right| + \left| \frac{\min [X_r(t)] - \min [X_c(t)]}{\min [X_c(t)]} \right| \right\} \quad (24)$$

where  $ERP_{dis}$  is the measurement displacement peak error.

### B. ACCELERATION WAVEFORM REPRODUCTION TEST

First, the time-frequency hybrid integration algorithm can further improve the seismic acceleration waveform reproduction accuracy compared with the traditional integration algorithm through the reproduction test of the sinusoidal

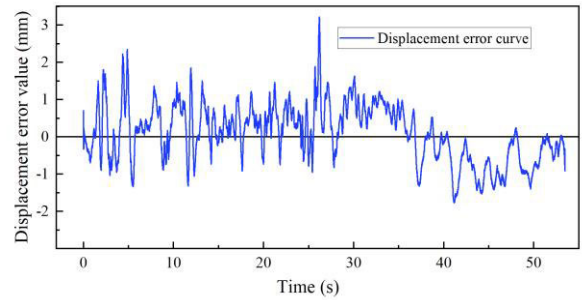


FIGURE 11. 110Gal El Centro displacement input and output error wave.

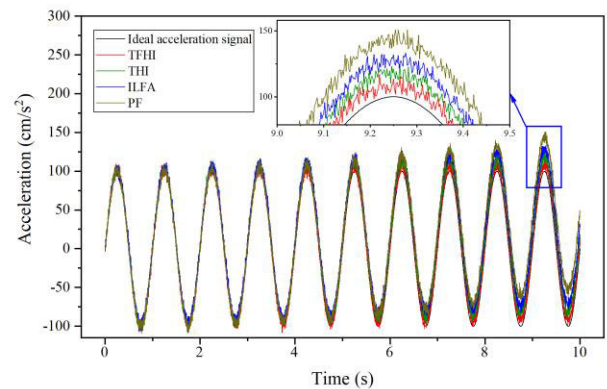


FIGURE 12. Acceleration recurrence curve under different integral algorithms.

acceleration signal with Gaussian noise. The signal's amplitude is  $100\text{cm/s}^2$ , and the frequency is 1Hz. The experimental results are shown in Fig. 12, from which it can be seen that the time-frequency hybrid integration algorithm has the highest acceleration waveform reproduction accuracy. Furthermore, it can be calculated that the acceleration peak error of the time-frequency hybrid integration reproduction is 0.222, which improves the reproduction accuracy by 27.29% compared with the traditional hybrid integration algorithm. Then, to further verify the reproducibility of the algorithm to the actual seismic acceleration signal, the 110Gal El Centro seismic acceleration signal was used for experiments. The acceleration waveform comparison graphs are shown in Fig. 13 and Fig. 14. The initial peak acceleration is 110gal, which occurs at 2.14s; the peak acceleration of the test value is 104.842gal, which occurs at 2.12s, and the maximum peak error rate is 4.92%, and the peak acceleration can be basically reproduced. It can be seen from the Fig. 13 that the error is mainly concentrated at the peak. The maximum peak error appears at 11.86s, as shown in the local enlargement of Fig. 14, and the error rate  $Err_{acc}$  is 38.87% when analyzed by the peak error rate equation (25), while the regular peak error rate is controlled by 15%.

$$Err_{acc} = \frac{A_r(t) - A_c(t)}{A_c(t)} \times 100\% \quad (25)$$

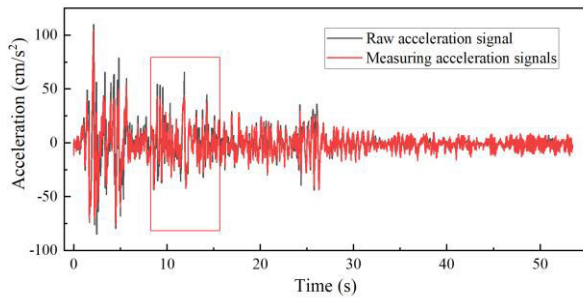


FIGURE 13. Comparison of accelerations of 110Gal El centro wave.

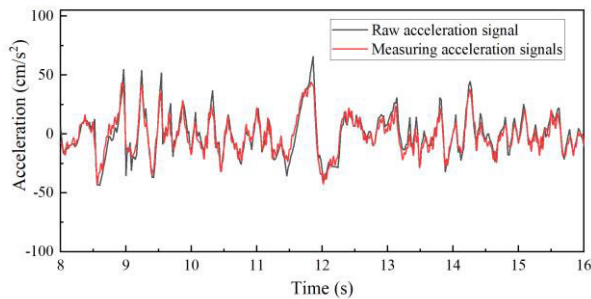


FIGURE 14. Local comparison of acceleration of 110Gal El centro wave.

where  $A_r(t)$  and  $A_c(t)$  are raw acceleration and measuring acceleration, respectively.

In summary, the shaker acceleration waveform follows well under the data processing of the time-frequency hybrid integration algorithm. Due to the equipment's limitation and noise, there is a certain degree of error in the experimental results. However, the accuracy of acceleration reproduction has been significantly improved.

## V. CONCLUSION

This paper proposes an algorithm to improve the accuracy of acceleration waveform reproduction in seismic simulation shaker tests: the time-frequency hybrid integration algorithm. It can be seen from the numerical simulation that the displacement obtained from the quadratic integration of the time-frequency hybrid integration algorithm is more consistent with the ideal displacement than the PF algorithm, the ILFA algorithm and the THI algorithm. The ERP and ERS of the displacement obtained by the time-frequency hybrid integration algorithm are reduced by 0.067 and 0.071, respectively, compared with the traditional hybrid integration, and the corresponding performance improvement rates of  $R_{ERP}$  and  $R_{ERS}$  are 31.75% and 26.01%, respectively. The shaking table test was conducted using the displacement obtained by the time-frequency hybrid integration algorithm: when the acceleration signal is sinusoidal, the acceleration waveform reproduction accuracy is improved by 27.29% compared with the traditional hybrid integration; when the acceleration is the actual seismic acceleration, the maximum peak error rate is 4.92%, and the seismic acceleration reproduction accuracy is higher. The above experiments show that the algorithm can

further improve the shaking table reproduction accuracy, and the algorithm has value for shaking table test research. At the same time, the principle and code of this algorithm are simple and readable. The research results are of great engineering relevance for exploring the seismic performance of building structures, position determination during aerial operation of UAVs, velocity and displacement estimation in inertial navigation systems, and micro-displacement measurements of roads and bridges.

## ACKNOWLEDGMENT

The authors would like to thank those who have granted them invaluable instructions during the process of thesis writing.

## REFERENCES

- [1] C. Geiß and H. Taubenböck, "Remote sensing contributing to assess earthquake risk: From a literature review towards a roadmap," *Natural Hazards*, vol. 68, no. 1, pp. 7–48, Aug. 2013.
- [2] J. Dai, Z.-D. Xu, P.-P. Gai, and Z.-W. Hu, "Optimal design of tuned mass damper inerter with a Maxwell element for mitigating the vortex-induced vibration in bridges," *Mech. Syst. Signal Process.*, vol. 148, Feb. 2021, Art. no. 107180.
- [3] J. Dai, Z.-D. Xu, Y.-Q. Guo, and C. Yang, "Hybrid seismic isolation of vertical pressure vessels in CO<sub>2</sub> capture plant," *Structures*, vol. 39, pp. 17–28, May 2022.
- [4] Z.-D. Xu, Y. Yang, and A.-N. Miao, "Dynamic analysis and parameter optimization of pipelines with multidimensional vibration isolation and mitigation device," *J. Pipeline Syst. Eng. Pract.*, vol. 12, no. 1, Feb. 2021, Art. no. 04020058.
- [5] R. Ozelik, B. Binici, and O. Kurç, "Pseudo dynamic testing of an RC frame retrofitted with Chevron braces," *J. Earthq. Eng.*, vol. 16, no. 4, pp. 515–539, May 2012.
- [6] Y. Zou, H. Liu, L. Jing, and J. Cui, "A pseudo-static method for seismic responses of underground frame structures subjected to increasing excitations," *Tunnelling Underground Space Technol.*, vol. 65, pp. 106–120, May 2017.
- [7] G. Magliulo, V. Pentangelo, G. Maddaloni, V. Capozzi, C. Petrone, P. Lopez, R. Talamonti, and G. Manfredi, "Shake table tests for seismic assessment of suspended continuous ceilings," *Bull. Earthq. Eng.*, vol. 10, no. 6, pp. 1819–1832, Dec. 2012.
- [8] R. Han and X. Zhao, "Shaking table tests and validation of multi-modal sensing and damage detection using smartphones," *Buildings*, vol. 11, no. 10, p. 477, Oct. 2021.
- [9] H. Ren, Q. Fan, and Z. Lu, "Shaking table test and parameter analysis on vibration control of a new damping system (PDAL)," *Buildings*, vol. 12, no. 7, p. 896, Jun. 2022.
- [10] P. Martinelli and F. C. Filippou, "Simulation of the shaking table test of a seven-story shear wall building," *Earthq. Eng. Struct. Dyn.*, vol. 38, no. 5, pp. 587–607, Apr. 2009.
- [11] H. Li, Z. Xu, D. Gomez, P. Gai, F. Wang, and S. J. Dyke, "A modified fractional-order derivative Zener model for rubber-like devices for structural control," *J. Eng. Mech.*, vol. 148, no. 1, Jan. 2022, Art. no. 04021119.
- [12] A. Ansari, A. Noorzad, and M. Zare, "Application of wavelet multi-resolution analysis for correction of seismic acceleration records," *J. Geophys. Eng.*, vol. 4, no. 4, pp. 362–377, Dec. 2007.
- [13] W. Zheng, D. Dan, W. Cheng, and Y. Xia, "Real-time dynamic displacement monitoring with double integration of acceleration based on recursive least squares method," *Measurement*, vol. 141, pp. 460–471, Jul. 2019.
- [14] J. Kim, L. Kim, and H. Sohn, "Autonomous dynamic displacement estimation from data fusion of acceleration and intermittent displacement measurements," *Mech. Syst. Signal Process.*, vol. 42, nos. 1–2, pp. 194–205, Jan. 2014.
- [15] W. Chen, B. Wang, and X. Hu, "Acceleration signal processing by numerical integration," *J. Huazhong Univ. Sci. Technol., Natural Sci. Ed.*, vol. 38, no. 1, pp. 1–4, 2010.
- [16] H. Zhu, Y. Zhou, and Y. Hu, "Displacement reconstruction from measured accelerations and accuracy control of integration based on a low-frequency attenuation algorithm," *Soil Dyn. Earthq. Eng.*, vol. 133, Jun. 2020, Art. no. 106122.

- [17] Y. H. Hong, S. G. Lee, and H. S. Lee, "Design of the FEM-FIR filter for displacement reconstruction using accelerations and displacements measured at different sampling rates," *Mech. Syst. Signal Process.*, vol. 38, no. 2, pp. 460–481, Jul. 2013.
- [18] H. S. Lee, Y. H. Hong, and H. W. Park, "Design of an FIR filter for the displacement reconstruction using measured acceleration in low-frequency dominant structures," *Int. J. Numer. Methods Eng.*, vol. 82, no. 4, pp. 403–434, Apr. 2010.
- [19] S. A. Odhano, R. Bojoi, S. G. Rosu, and A. Tenconi, "Identification of the magnetic model of permanent-magnet synchronous machines using DC-biased low-frequency AC signal injection," *IEEE Trans. Ind. Appl.*, vol. 51, no. 4, pp. 3208–3215, Jul. 2015.
- [20] A. Suzuki and K. Ohnishi, "Frequency-domain damping design for time-delayed bilateral teleoperation system based on modal space analysis," *IEEE Trans. Ind. Electron.*, vol. 60, no. 1, pp. 177–190, Jan. 2013.
- [21] Q. Zhang and X. Y. Zheng, "Walsh transform and empirical mode decomposition applied to reconstruction of velocity and displacement from seismic acceleration measurement," *Appl. Sci.*, vol. 10, no. 10, p. 3509, May 2020.
- [22] B. Lotfi and L. Huang, "An approach for velocity and position estimation through acceleration measurements," *Measurement*, vol. 90, pp. 242–249, Aug. 2016.
- [23] X. Kong, W. Yang, H. Luo, and B. Li, "Application of stabilized numerical integration method in acceleration sensor data processing," *IEEE Sensors J.*, vol. 21, no. 6, pp. 8194–8203, Mar. 2021.
- [24] F. Liu, S. Gao, and S. Chang, "Displacement estimation from measured acceleration for fixed offshore structures," *Appl. Ocean Res.*, vol. 113, Aug. 2021, Art. no. 102741.
- [25] A. Ansari, A. Noorzad, H. Zafarani, and H. Vahidifard, "Correction of highly noisy strong motion records using a modified wavelet denoising method," *Soil Dyn. Earthq. Eng.*, vol. 30, no. 11, pp. 1168–1181, Nov. 2010.
- [26] Y.-Q. Guo, Z.-Y. Li, X.-L. Yang, and J.-B. Li, "Research on shaking table test of earthquake simulation based on hybrid integration algorithm," *IEEE Access*, vol. 8, pp. 208961–208968, 2020.
- [27] D. M. Boore and J. J. Bommer, "Processing of strong-motion accelerograms: Needs, options and consequences," *Soil Dyn. Earthq. Eng.*, vol. 25, no. 2, pp. 93–115, Feb. 2005.



**HAN-QI ZHANG** is currently pursuing the M.A.Eng. degree in seismic simulation shaking table control technology with the College of Mechanical and Electronic Engineering, Nanjing Forestry University. His research interests include motor control, embedded systems, intelligent control algorithms, and machine learning.



**YI-NA WANG** received the Ph.D. degree in detection technology and automation devices from Shandong University, Jinan, China, in 2021. Since 2021, she has been a Lecturer with the College of Mechanical and Electronic Engineering, Nanjing Forestry University, China. Her research interests include intelligent detection, automation detection devices, and spectral analysis technology.



smart materials and structures, and vibration control.

**YING-QING GUO** received the Ph.D. degree from Southeast University, Nanjing, China, in 2010. She has been a Visiting Scholar with North Carolina State University and University of Illinois at Urbana Champaign, USA, for three years. She is currently a Professor with the College of Mechanical and Electronic Engineering, Nanjing Forestry University, China. She is the author of two books, more than 80 articles, and more than 60 inventions. Her research interests include intelligent control,



**JUN DAI** received the Ph.D. degree in civil engineering from Southeast University, Nanjing, China, in 2020. Since 2021, he has been an Assistant Professor with the School of Civil Engineering, Southeast University. He has published more than 30 journal articles. His research interests include structural vibration control, structural dynamics, and nonlinear system identification.

...